

# Characterizing Swirl Strength and Recirculation Zone Formation in Tangentially Injected Isothermal Flows

R. Sharma and M. Kumar<sup>†</sup>

Department of Mechanical Engineering, Indian Institute of Technology Delhi, New Delhi, 110016, India

<sup>†</sup>Corresponding Author Email: [kmayank@mech.iitd.ac.in](mailto:kmayank@mech.iitd.ac.in)

(Received April 25, 2022; accepted November 9, 2022)

## ABSTRACT

This paper presents a computational study characterizing the swirl intensity distribution and Internal Recirculation Zone (IRZ) formed in a cylindrical domain with tangential injections and isothermal flow. The range of inlet boundary conditions investigated is  $5^\circ$  to  $25^\circ$  for the injection angle and 7190 to 100711 for the bulk flow Reynolds number. The evolution of swirl intensity is presented with and without incorporating effects of the accompanying pressure variations. The Shear Stress Transport (SST)  $k-\omega$  is used to model turbulence. Results show that the Swirl strength created by such tangential injections strongly depends on the injection angle but does not vary with bulk flow Reynolds number ( $Re$ ), except for low  $Re$  values. The swirling flow is shown to result in IRZ formation at injection angles  $6^\circ$  and above or when asymptotic value of the maximum Swirl Number in the domain exceeds approximately 0.6, same as the transition value of inlet Swirl Number in swirling flows with axial injections. The IRZ length increases with injection angle and varies with  $Re$  for lower values of  $Re$  at a given injection angle but asymptotes for higher values above 40000. The conventional Swirl Number rises rapidly downstream of the injection plane followed by a slow decline. On the other hand, an alternative Swirl Number, which incorporates the gauge pressure variation, shows slow and consistent decay all the way downstream of the injection plane. The Swirl Number incorporated with gauge pressure term subsumes interconversions between the axial momentum and pressure in the regions of vortex breakdown and IRZ formation, thereby presenting an alternative picture of swirl intensity evolution in swirling flows.

**Keywords:** IRZ; Swirling flow; Tangentially injected burner; Swirl burner and Swirl number.

## NOMENCLATURE

$D$	diameter of the domain	$S_p$	Swirl number considering static pressure
$G_x$	axial flux of linear momentum	$T$	mean temperature
$G_x'$	total axial flux of linear momentum	$T'$	fluctuating temperature component
$G_\theta$	axial flux of angular momentum	$U$	axial velocity component
$L$	length of the cylindrical domain	$u_i$	average velocity components
$p$	pressure	$u_i'$	fluctuating velocity component
$P$	static pressure	$W$	tangential velocity component
$R$	exit radius	$\lambda$	gas-phase thermal conductivity
$Re$	Reynolds number	$\rho$	density of the fluid
$S$	Swirl number	$\delta_{ij}$	$ij^{th}$ component of Kronecker-delta tensor
$S_h$	source term due to radiation, homogeneous reactions, and exchange of energy between phases	$\mu$	dynamic viscosity
		$\Phi$	viscous dissipation

## 1. INTRODUCTION

The study of swirling and rotating flows is of great importance in various applications such as gas turbine engines (Syred and Beer 1974), cyclone separators

(Beér *et al.* 1984; Gupta *et al.* 1984), swirl burners and furnaces (Syred and Beer 1974; Benesch and Kremer 1985; Gaikwad *et al.* 2017; Mansouri and Boushaki 2018), heat transfer enhancement in some designs of heat exchangers (Bezaatpour and Goharkhah 2020), efficiency improvement in thermal systems (Zhao *et*

*al.* 2019, 2020; Zhao and Song 2021) and aircraft wingtip vortices (Gerz and Ehret 1997). This paper focuses on modeling turbulent swirling flows in confined domains, as relevant to swirl burners and tangentially-injected burners which utilize such flows to remarkably boost combustion efficiency and stability. The present work focuses on isothermal flow modeling, and the analysis will be extended to reacting flows in a subsequent paper. The presence of swirl, which involves rotating or circulating flow about the central axis of the confined domain, often in a helical shape, results in axial and radial pressure gradients (Gupta *et al.* 1984). When sufficiently large, these gradients results in negative axial velocities, thus establishing an Internal Recirculation Zone (IRZ) along the axis of rotation. IRZ remarkably augments the mixing between the colder reactants and the hot products, resulting in greater flame stability and compact size of combustion zone (Gupta *et al.* 1984; Villasenor and Escalera 1998).

Swirling flows in a confined domain can be classified into two types depending upon how swirl is imparted: first, using an axial swirling injection in Swirl Burners (SBs) and second, with the help of tangential injections from the furnace walls in Tangentially-Injected Burners (TIBs). For confined swirling flows in TIBs, the swirl can also be generated using the rotation of cylinder walls (sidewall or endwall) (Escudier 1984; Brown and Lopez 1990a,b), and single or multiple point injections (Escudier *et al.* 1980; Wang and Yang 2018; Wang *et al.* 2018). Characterizing swirling flows in TIBs with multiple point injections is the focus of this work.

The fluid dynamics of turbulent swirling flows involve multiple complex phenomena and concomitant flow structures, e.g., swirl generation, asymmetric vortex cores, Precessing Vortex Cores (PVCs), vortex breakdown, IRZs, instabilities and other coherent structures (Syred and Beer 1974; Gupta *et al.* 1984; Alekseenko *et al.* 1999; Doherty 2001; Serre and Bontoux 2002; Cary and Darmofal 2003; Al-Abdeli and Masri 2015; Wang and Yang 2018; Wang *et al.* 2018). These factors increase the complexity of controlling the flow and combustion. For low swirl intensity flows with no IRZ, the vortex core can either be aligned along the axis of symmetry in a straight line or occur in the shape of a helix with both steady and unsteady realizations (Escudier *et al.* 1980; Alekseenko *et al.* 1999; Mansouri and Boushaki 2018). On the other hand, for high swirl intense flows (typically  $S > 0.6$ ), vortex breakdown takes place and induces an internal recirculation zone (Syred and Beer 1974; Escudier *et al.* 1980; Gupta *et al.* 1984). However, the shape and size of the exhaust, inlet and the domain affects the critical value of  $S$  for vortex breakdown (Gupta *et al.* 1984). For characterizing the flow behavior and structures in such swirling flows under isothermal conditions, several experimental and computational studies have been conducted over the past decades that are available in the open literature. The present discussion includes relevant and significant studies on both SBs (Syred and Beer 1974; Gupta *et al.* 1984; Ahmed and Nejad 1992; Ahmed, 1998; Villasenor and Escalera, 1998; Doherty, 2001; Stone and Menon 2001; Serre and Bontoux, 2002;

Cary and Darmofal 2003; Wang *et al.* 2004; Al-Abdeli and Masri 2015; Mansouri and Boushaki 2018) and TIBs (Harvey 1962; Escudier *et al.* 1980; Alekseenko *et al.* 1999; Chen *et al.* 2017; Wang and Yang 2018; Wang *et al.* 2018).

The Swirl intensity or Swirl strength in a flow is characterized by the non-dimensional parameter called Swirl Number (Gupta *et al.* 1984). Two different definitions are possible for the Swirl Number in isothermal flows (Syred and Beer 1974) :

$$S_p = \frac{G_\theta}{G'_x R} \quad (1)$$

$$S = \frac{G_\theta}{G_x R} \quad (2)$$

Where,

$$G_\theta = \int_0^R W r \rho U 2\pi r dr$$

$$G'_x = \int_0^R U \rho U 2\pi r dr + \int P. 2\pi r dr$$

$$G_x = \int_0^R U \rho U 2\pi r dr$$

The Swirl Number expression ( $S_p$ ) in Eq. (1) normalizes the axial flux of angular momentum via the summation of the axial flux of axial momentum and the gauge pressure force. Whereas, the Swirl Number,  $S$ , in Eq. (2) excludes the gauge pressure term in the denominator (Syred and Beer 1974). Nearly all swirling flow studies in the literature have used the form of Swirl Number as shown in Eq. (2) to characterize the Swirl strength (Weber *et al.* 1990; Xia *et al.* 1998; Anacleto *et al.* 2003; Wang *et al.* 2004). The Swirl Number expressed in Eq. (1) is argued to be a better alternative for describing the evolution of swirl strength in the cases presented in this work.

Syred and Beer (1974), Gupta *et al.* (1984), Al-Abdeli and Masri (2015) summarized number of studies on isothermal confined swirling flows in SB-type and Cyclone combustor-type (with tangential and axial injection simultaneously) geometries. They summarized that the Swirl Number,  $S$ , in most SB geometries falls in the range 0.6 to 2.5 and the IRZ formation is not observed for values of  $S$  below 0.6 for isothermal flows with straight exit. The length of IRZ was also observed to increase with  $S$  up to a value of 1.5, beyond which further increment in  $S$  shortens the IRZ length and broadens the corresponding radius substantially, for SB geometry. The critical value of IRZ initiation depends upon various factors apart from the Swirl Number, like central hub size, exhaust shape, isothermal or reacting flow and sudden expansion effect (Gupta *et al.* 1984).

Wang *et al.* (2004), Ahmed and Nejad (1992) and Ahmed (1998) conducted isothermal studies of swirling flow on the same SB geometry with sudden expansion and showed that the swirling flow shrank the corner recirculation length more effectively in comparison with purely axial flow, and increasing the Swirl strength shifted the IRZ upstream, with further increment making the IRZ oscillatory in nature. Boushaki *et al.* (2017) visualized the evolution of

turbulent isothermal swirling flows in coaxial SB geometry and demonstrated the asymmetrical nature of swirling flow therein. Mansouri and Boushaki (2018) worked on the same coaxial SB design with Swirl Number of 1.4 to experimentally and numerically observe the isothermal and reacting swirling flow structures.

Furthermore, the evolution of Swirl strength along the domain has been previously analyzed for both SB (Weber *et al.* 1990; Ahmed and Nejad 1992) and TIB geometries (Chen *et al.* 2017; Wang *et al.* 2018). Among these, Chen *et al.* (2017), Ahmed and Nejad (1992) and Weber *et al.* (1990) reported the Swirl strength distribution in their respective domains. Whereas Wang *et al.* (2018) observed the Swirl strength distribution and attempted to draw a relationship with the corresponding IRZ length. Moreover, Wang *et al.* (2018) also reported a weak dependency of Swirl strength on Re for laminar flows. However, these studies do not discuss the physical reasoning behind the observed distributions and dependencies. Hence, there is scope for deeper investigation into the physical reasoning behind the observed distributions.

Our comprehensive review of the available literature on isothermal confined swirling flows and the associated fluid mechanical phenomena in both SBs and TIBs makes it sufficiently clear that:

- Nearly all studies use the Swirl Number ( $S$ ) instead of  $S_p$  to characterize the Swirl strength.
- Although a few studies focus on analyzing the Swirl strength distribution through the domain, they do not provide any coherent reasoning behind the observed distribution and whether  $S$  is the ideal parameter to characterize the Swirl strength.
- The quantum of research conducted on SBs far outweighs that on TIBs, including both experimental and analytical investigations.

Accordingly, the present work attempts to bridge the aforementioned gaps and explore the range of flow phenomena encountered in TIBs with the aid of suitable parametric simulation studies. This paper presents our investigations into the isothermal swirling

flow characteristics in a simple cylindrical domain with tangential injection.

## 2. PHYSICAL MODEL

The swirling flow behaviour depends intricately on the domain configuration like convergent-divergent exit, sudden expansion, swirler type etc. (Gupta *et al.* 1984). This study adopts the simple cylindrical domain of 0.3 m diameter ( $D$ ) to avoid any additional flow complexities caused by the geometry and explore the fundamental flow as shown in Fig. 1. A sufficiently long domain with  $L/D$  ratio of 10 is chosen to allow complete resolution and full development of downstream swirling flow patterns. Here, the length  $L$  is extent of the domain downstream from the injection plane as shown in Fig. 1.

The geometry has four square-shaped injectors, each with a hydraulic diameter of  $0.15D$ , placed symmetrically on the peripheral wall of the cylindrical domain, at the height of  $1.67D$  from the base to minimize the impact of the bottom wall on the flow. The cylindrical domain is discretized into fully structured 516K mesh elements, as depicted in Fig. 2. The computational domain is discretized through the O-grid method with an orthogonal quality of 0.79 and maximum aspect ratio of 20. The mesh has size gradients along the axial and radial direction for appropriate flow resolution and smooth convergence. The first grid distance from the wall is set to 0.0015 m, which gives the range of  $y^+$  as 10 to 40 across the Re variation considered.

Several simulations are performed by changing the inlet boundary conditions on the cylindrical domain using a validated turbulence model. The injection angles investigated in this work range from  $5^\circ$  to  $25^\circ$ , the reasoning for this selection being elaborated later in the results and discussion section. Since the current work focuses on swirling flows in the turbulent regime only, the range of mass flow rates investigated is such that the resultant flow lies beyond the laminar and transition regime. The injection flow rates investigated range from 0.005 kg/s to 0.07 kg/s with corresponding bulk flow Reynolds number (Re) ranging from 7190 to 100711. All the subsequent analysis in this paper will

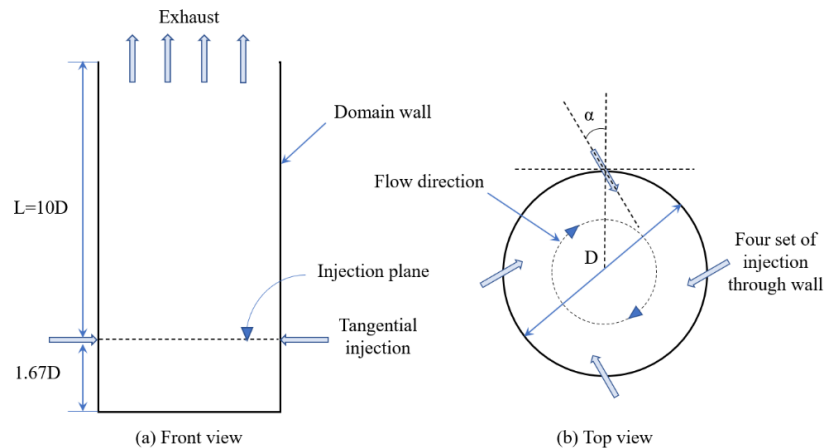


**Fig. 1. Schematic diagram of the cylindrical domain with four symmetric tangential injectors,  $\alpha$  is the injection angle.**

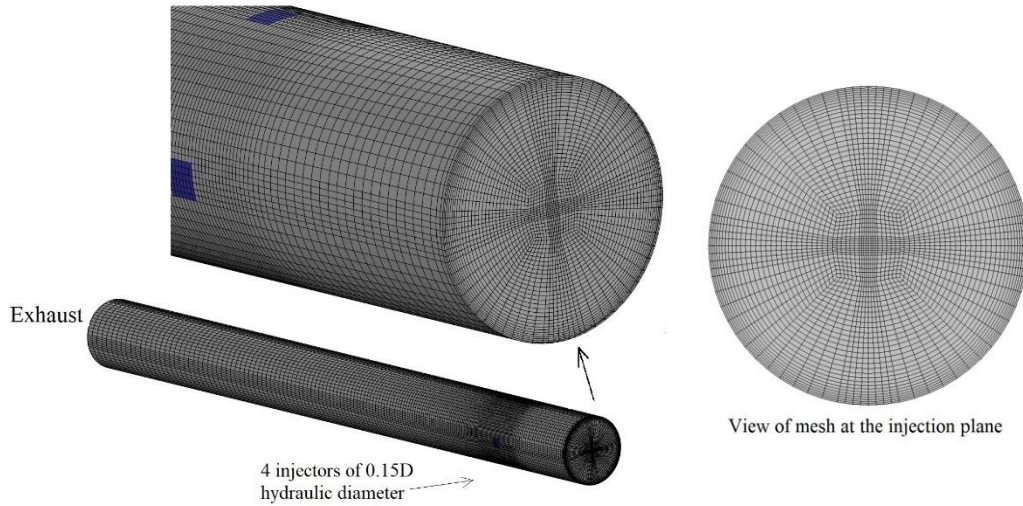


**Fig. 2. Discretized cylindrical domain with four square injectors.**

include  $Re$  as the flow rate input boundary condition.

The inlet and outlet boundary conditions are mass flow inlet and pressure outlet, respectively, along with the turbulent intensity set at 5% and hydraulic diameter of 0.04417 m. The turbulent kinetic energy and axial velocity at a point 0.5 m from the injection on the central axis of the domain are monitored simultaneously along with the default residual monitors for convergence.

### 3. GOVERNING EQUATIONS AND NUMERICAL METHODS

All cases in this work are simulated using the SST  $k-\omega$  RANS turbulence model on the Ansys Fluent 19.2 platform (Ansys user manual 19.2). Pressure velocity coupling is achieved via the inbuilt coupled scheme, pressure discretization via PRESTO, whereas QUICK is used for the discretization of all other parameters. The flow is simulated by solving the steady-state forms of the governing equations for mass, momentum and energy. Solving the energy equation is necessitated because the ideal gas assumption is selected for the working fluid instead of constant density in Ansys Fluent.

$$\frac{\partial}{\partial x_i}(\rho u_i) = 0 \quad (3)$$

$$\frac{\partial(\rho u_i u_j)}{\partial x_j} = -\frac{\partial p}{\partial x_i} + \frac{\partial}{\partial x_j} \left\{ \mu \left( \frac{\partial u_i}{\partial x_j} + \frac{\partial u_j}{\partial x_i} - \frac{2}{3} \delta_{ij} \frac{\partial u_k}{\partial x_k} \right) \right\} + \frac{\partial}{\partial x_j}(-\rho \overline{u_i' u_j'}) \quad (4)$$

$$\frac{\partial(\rho c_p u_i T)}{\partial x_i} = \frac{\partial}{\partial x_i} \left( \lambda \frac{\partial T}{\partial x_i} - c_p \rho \overline{u_i' T'} \right) \quad (5)$$

The numerical results qualify the grid independence check, as shown in Fig. 3, which presents the comparative distribution of centerline axial velocity. The comparative plot has results of the simulated cases for four different mesh sizes at the same boundary conditions (47500 bulk flow  $Re$  and  $10^\circ$  injection angle). The plot shows that the simulation results are independent of mesh size for most of the domain

between 516K and 1.37M meshes. Hence, the 516K mesh is used for all the cases in the current study.

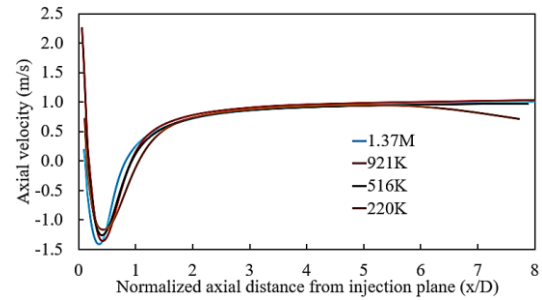


**Fig. 3: Distribution of axial velocity on the central axis of the domain for three different mesh resolutions.**

### 4. MODEL VALIDATION

As stated in the introduction section, there are very few studies on TIBs in the open literature. Furthermore, no experimental test case could be found in the literature which could be used to validate our model for swirling flows in a tangentially fired configuration. Since SBs and TIBs have swirling flow in common and standardized test cases for validating turbulent flows in SBs do exist in the literature, the viable alternative of validating our turbulence model against one such experimental study is taken. The apparent extrapolation is that if our model yields satisfactory comparisons with the experimental data of the SB test case, it expectedly captures the general aspects of swirling flow physics and can also be applied to TIB configurations with reasonable accuracy.

Accordingly, an experimental study on coaxial dump combustor for isothermal swirling flow operating in SB configuration by Ahmed and Nejad (1992), as shown in Fig. 4 (a), is used for model validation. Flow velocity profiles in the domain are measured using Laser Doppler Velocimeter (LDV) arrangement. Our simulation domain for the validation is discretized with  $8.20 \times 10^5$  fully structured mesh elements and a minimum orthogonal quality of 0.22, as shown in Fig.

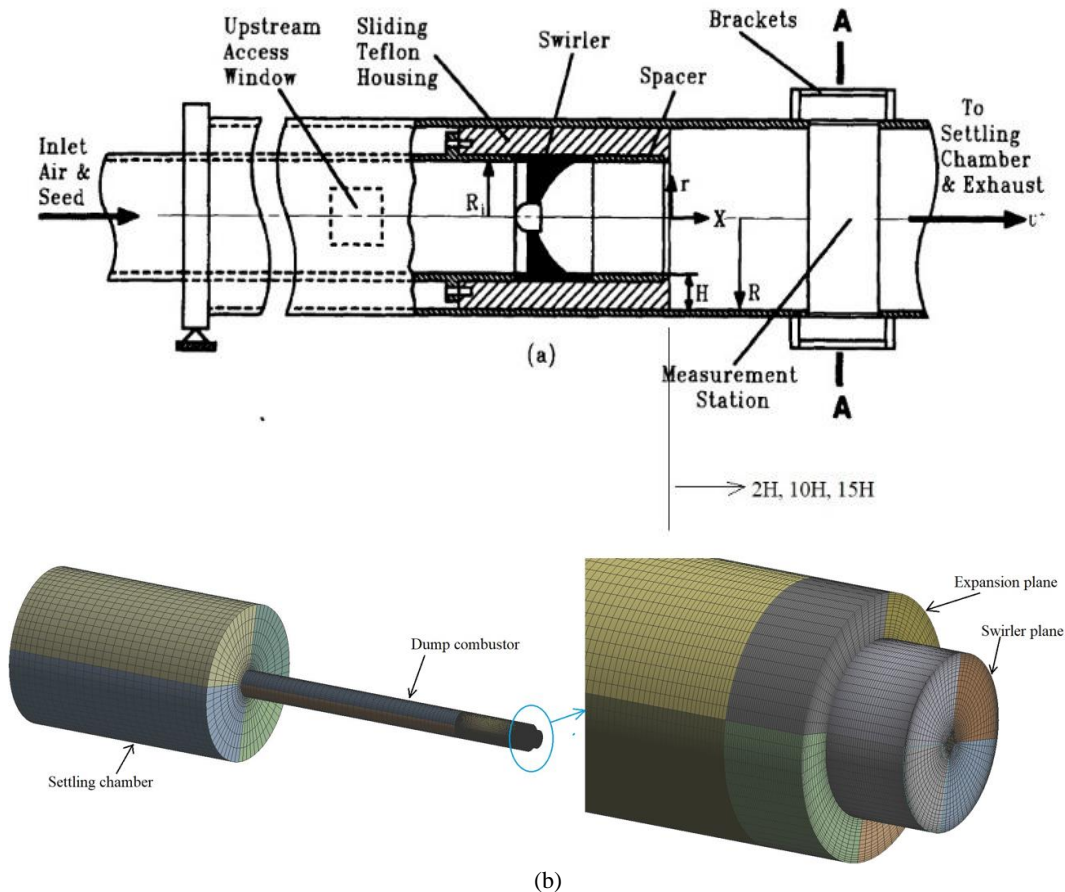


**Fig. 4. (a) Illustrative diagram of the dump combustor with swirler and inlet pipe arrangement (b) View of discretized SB geometry mesh in current validation case.**

4 (b). In this experimental study, guide vanes were used to create swirling flow at the combustor inlet with Swirl Number of 0.4. The Reynolds number based on the bulk flow in the inlet pipe is  $1.25 \times 10^5$ . Any other geometrical or operational parameters are the same as provided in the reference (Ahmed and Nejad 1992).

Simulating turbulent swirling flows using RANS models is non-trivial and researchers have pointed toward models like the  $k-\epsilon$  model (RNG and Realizable), which works well for low intensity swirling flows (Chen *et al.* 2017; Mansouri and Boushaki 2018). These models are not likely to predict the highly turbulent swirling flows accurately (Ko 2005). The Reynolds stress and the SST  $k-\omega$  models are found to give promising results for highly turbulent swirling flows (Ko 2005; Gaikwad *et al.* 2017).

As the inlet Reynolds number falls in the turbulent flow region, the case is simulated and compared with experimental data (Ahmed and Nejad no date; Ahmed and Nejad 1992) by assuming three different turbulence models, i.e., Reynolds stress, RNG  $k-\epsilon$  (with swirl dominated flow), and SST  $k-\omega$  model. To ensure convergence, the turbulent kinetic energy and axial velocity along with the residuals at a point 0.1 m ahead of the dump combustor's inlet plane are monitored.

The predicted axial velocity profiles along the radial and axial directions using the three turbulence models

are compared with the experimental data at the axial locations of 2H, 15H, and the geometry centerline, as shown in Fig. 2, where H is 0.0254 m. The graphs in Fig. 5 show that the SST  $k-\omega$  model gives better agreement with the experimental data compared to the Reynolds stress and RNG  $k-\epsilon$  (with swirl dominated flow) models. The excellent comparisons indicate that the SST  $k-\omega$  model can be expected to capture the steady-state flow field and the associated physics in swirling flows with reasonable accuracy.

## 5. RESULTS AND DISCUSSION

For the given configuration, the flow evolution is governed by the injection angle and mass flow rate. In the following analysis, the evolution of swirling flow will be discussed first by analysing the development of swirl intensity parameters like  $S_P$  and  $S$ . After that, the different regimes in such flows will be discussed, which involve the formation, size, and shape of IRZ and its connection with the swirl intensity. The current analysis is limited to injection angles up to  $25^\circ$ , beyond which the reverse flow at the exit becomes increasingly dominant, even merging with the IRZ downstream of the injection.

### 5.1. Evolution of Swirl Intensity

In this section, the two alternative definitions of Swirl Number, namely  $S_P$  and  $S$ , are evaluated via Eq. (1) &

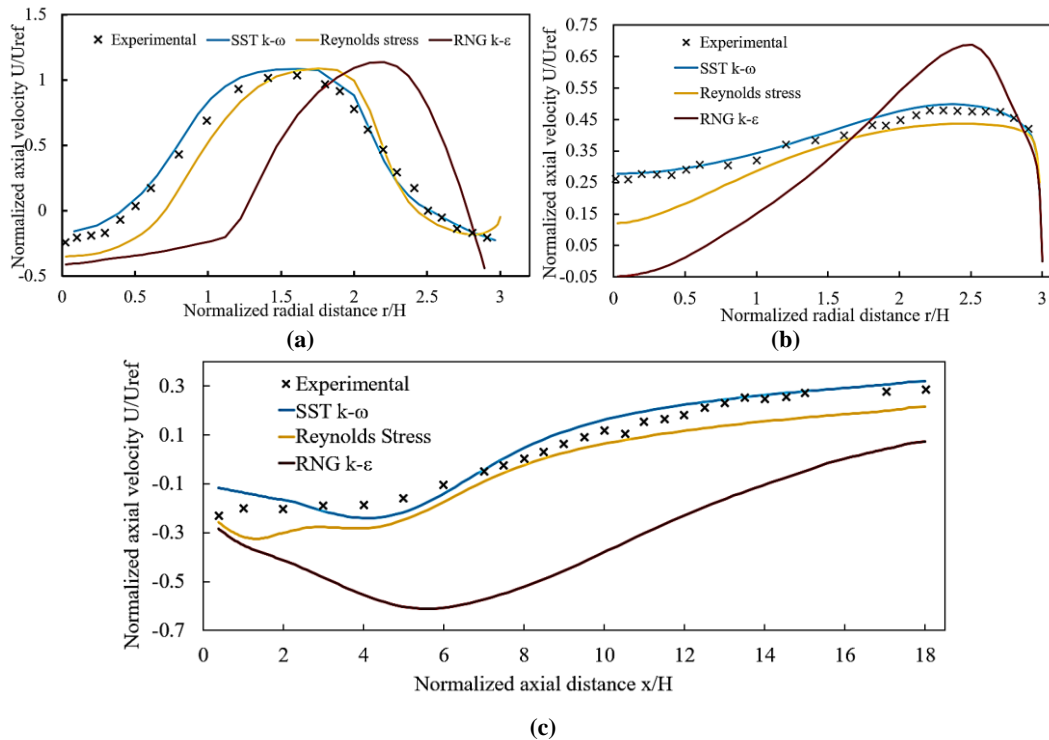


**Fig. 5. Distribution of predicted axial velocity, normalized by  $U_{ref}$  (19.2 m/s) for all turbulence models considered along with experimental data (a) at the plane  $2H$  distance, (b)  $15H$  distance from the combustor inlet and (c) along the central axis.**

(2) at various sections of the domain and compared. Fig. 6 & 7 show the distribution of  $S$  along the domain, whereas Fig. 9 shows the comparative plot of  $S_p$  and  $S$ . Across the range of inlet boundary conditions considered in the present work,  $S$  is observed to rise rapidly downstream of the injection plane and decrease gradually thereafter along the domain. Similar distribution of  $S$  has also been reported by Stone and Menon (2001), Ahmed and Nejad (1992), Benesch and Kremer (1985) and Chen *et al.* (2017) without providing any physical reasoning to explain these variations, as also discussed in the introduction section. The reason for the rapid rise immediately following the injection is the corresponding substantial decay in the axial flux of axial momentum, as seen in Fig. 6(a). Interestingly, this is also the region where vortex breakdown and IRZ formation takes place as detailed in the next section. While the axial momentum remains relatively unchanged thereafter, the angular momentum is observed to continuously decay till the exit. Accordingly, the gradual decay in Swirl Number, followed by the initial sharp increase, is due to the continuous decline in angular momentum caused by viscous effects.

The sharp drop of axial momentum downstream of the injection plane, observed in Fig. 6(a), can be further investigated from the comparison between the gradient of axial momentum and the gradient of area-weighted average static pressure as shown in Fig. 6(b). Observation shows that these quantities have comparable magnitude and opposite signs, thereby balancing each other in the region of interest just downstream of the injection plane. Therefore, there is rapid interconversion between pressure and axial

momentum in this region, and the same explains the sharp drop in axial momentum and the concomitant rise in pressure.

The preceding section discussed the axial distribution of Swirl Number and the contribution of the constituent physical terms to its observed variation. The contours of these individual terms have been presented at different cross sections in Fig. 7 to investigate their radial and tangential distributions. The first, second and third row of Fig. 7 show the contours of static gauge pressure, axial momentum and angular momentum, respectively, at five different sections. It is observed that the axial momentum and static gauge pressure terms have sharp gradients along the radial and tangential directions just downstream of the injection plane. These terms reach relatively stable values further downstream as depicted by the uniform 'light green' contours in the downstream sections. The very first section downstream of the injection displays sharp departures from the green background with opposite signs for the static gauge pressure and axial momentum terms, especially around the central region, indicating interconversion between these two terms present in the denominator of Swirl Number  $S_p$ . These departures subside and merge into the green background successively downstream. It should be noted that the radial and tangential gradients in the angular momentum term are relatively insignificant.

It is also interesting to observe the relatively steeper drop in  $S$  at the end of the domain for all injection angles above  $5^\circ$  in Fig. 8. This end effect is due to the formation of another reverse flow zone at the domain exit, except for the  $5^\circ$  injection angle, as detailed in the next section. The reverse flow zone results in a drop in

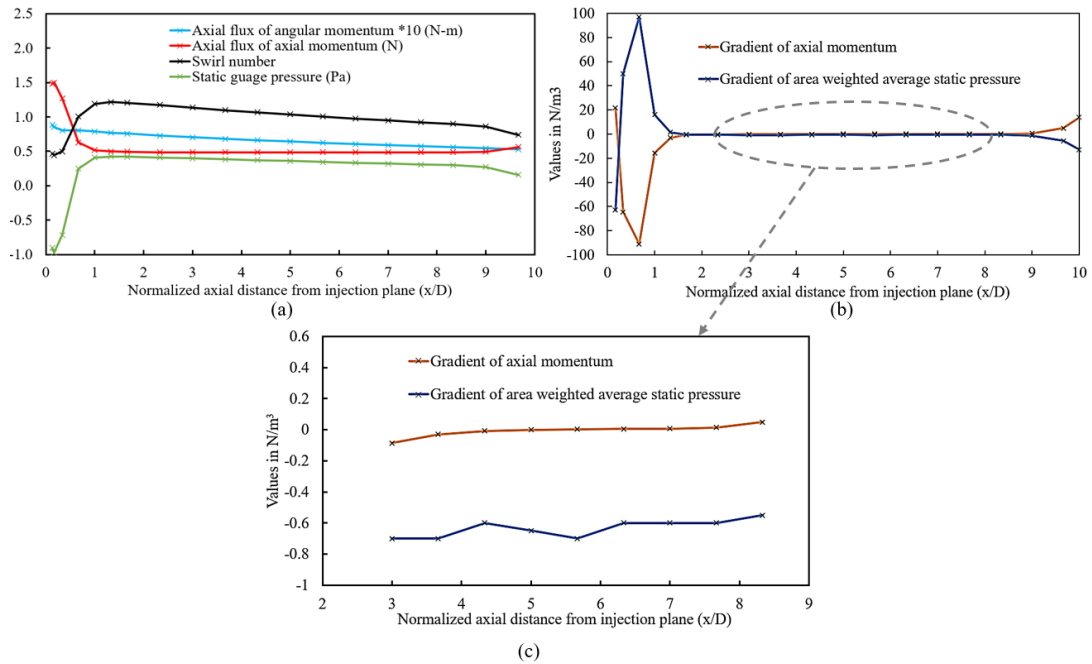


**Fig. 6. Distribution of (a) Swirl number ( $S$ ), Axial flux of axial momentum, axial flux of angular momentum and static gauge pressure, (b) Gradient of axial momentum and area-weighted average static pressure along with normalized axial distance for  $Re\ 71900$  and injection angle  $10^\circ$ , (c) Zoomed view of plot in Fig. 6(b) for specific range from  $3D$  to  $8.5D$ .**

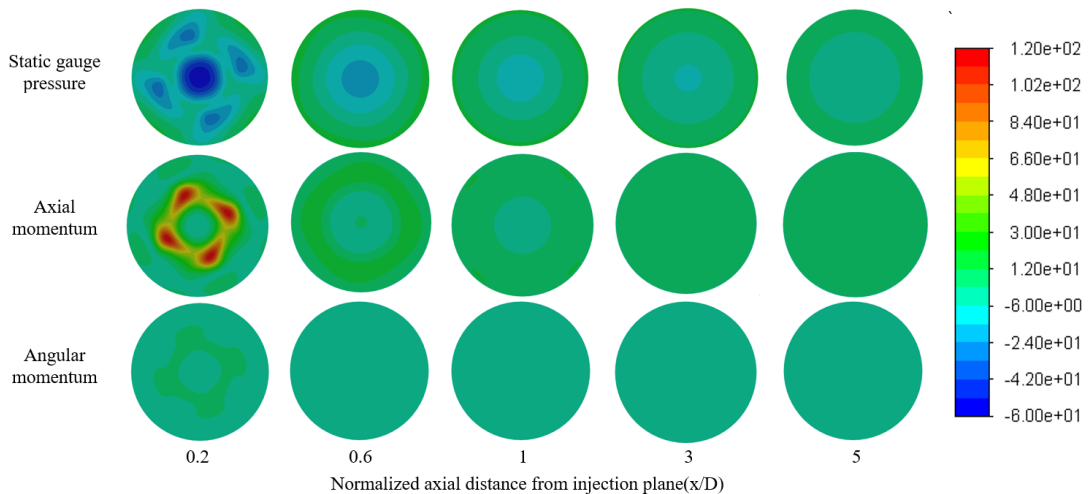


**Fig. 7. Contours of static gauge pressure ( $N/m^2$ ), axial momentum ( $N/m^2$ ) and angular momentum ( $N/m$ ) at the multiple sections of the domain for  $Re\ 71900$  and injection angle  $10^\circ$ .**

$S$ , owing to the interconversion between pressure and axial momentum, as already discussed.

The above explanation for the variations in  $S$  along the domain calls for investigating the variation of Swirl Number,  $S_P$ , along the domain since it has the addition of pressure and axial momentum in the denominator, expectedly resulting in the cancellation of their opposing trends. Fig. 9 shows the comparative plots of  $S_P$  and  $S$ , wherein  $S_P$  is observed to drop gradually and nearly in a linear fashion from the injection to the exhaust, in stark contrast with the  $S$  variation. Despite their contrasting patterns within the domain, the two Swirl Numbers attain the same value at the end as the gauge pressure vanishes at the domain exit. The overall variation of  $S_P$  is much better reflective of the corresponding variation in angular

momentum, as depicted in Fig. 6(a), throughout the domain and is unaffected by the interconversion between pressure and axial momentum that distinctly affected the variation of  $S$  in the regions of vortex breakdown and IRZ formation. Hence,  $S_P$  can be argued to be a better descriptor of the swirl intensity in swirling flows.

Figure 9 also shows that  $S_P$  drops more slowly than  $S$  through the domain after the initial jump in the latter. This can be explained by Fig. 6(c), a zoomed-in plot of Fig. 6(b). Figure 6(c) shows that the axial momentum remains almost unchanged, and there is a small consistent decay in the static gauge pressure in that region, which damps the effect of angular momentum decay in the expression of  $S_P$  in Eq. (1).

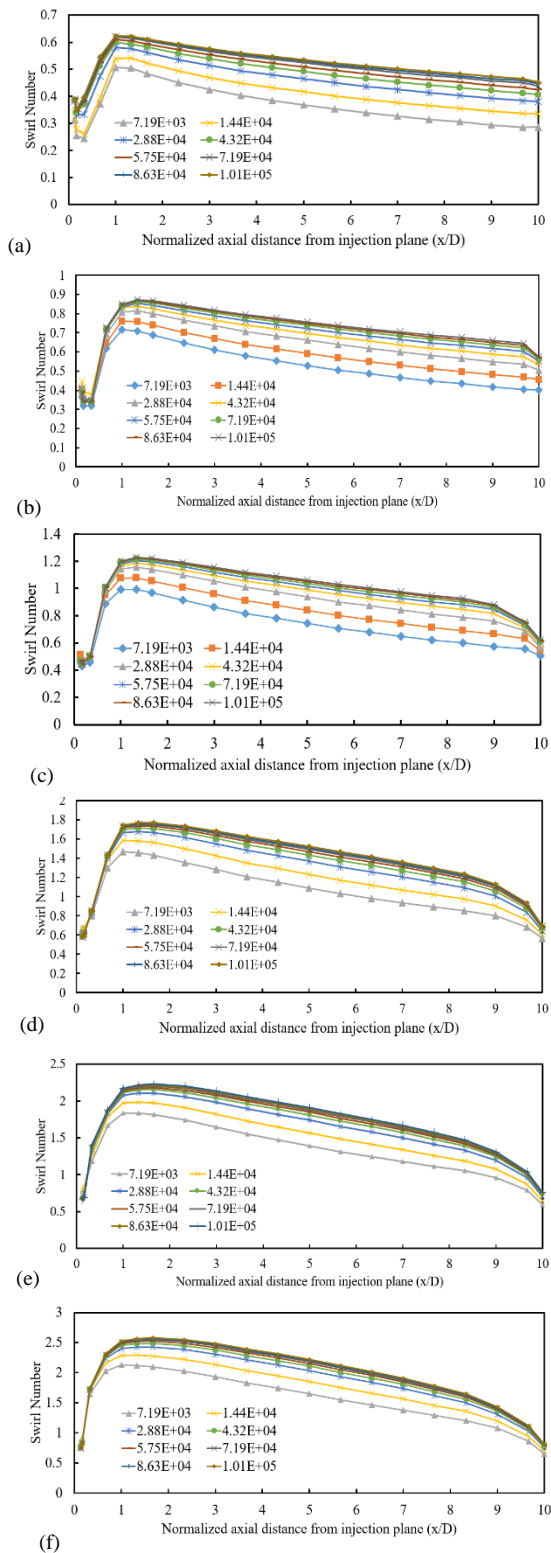


**Fig. 8: Distribution of Swirl number ( $S$ ) along with normalized axial distance for various bulk flow Reynolds number (mentioned in the legend) considered, for injection angles (a)  $5^\circ$  (b)  $7^\circ$  (c)  $10^\circ$  (d)  $15^\circ$  (e)  $20^\circ$  (f)  $25^\circ$**

### 5.2. Swirling Flow Regimes

Instead of looking at the variation of  $S$  and  $S_p$ , across the domain for all the cases as shown in Figures 8 and

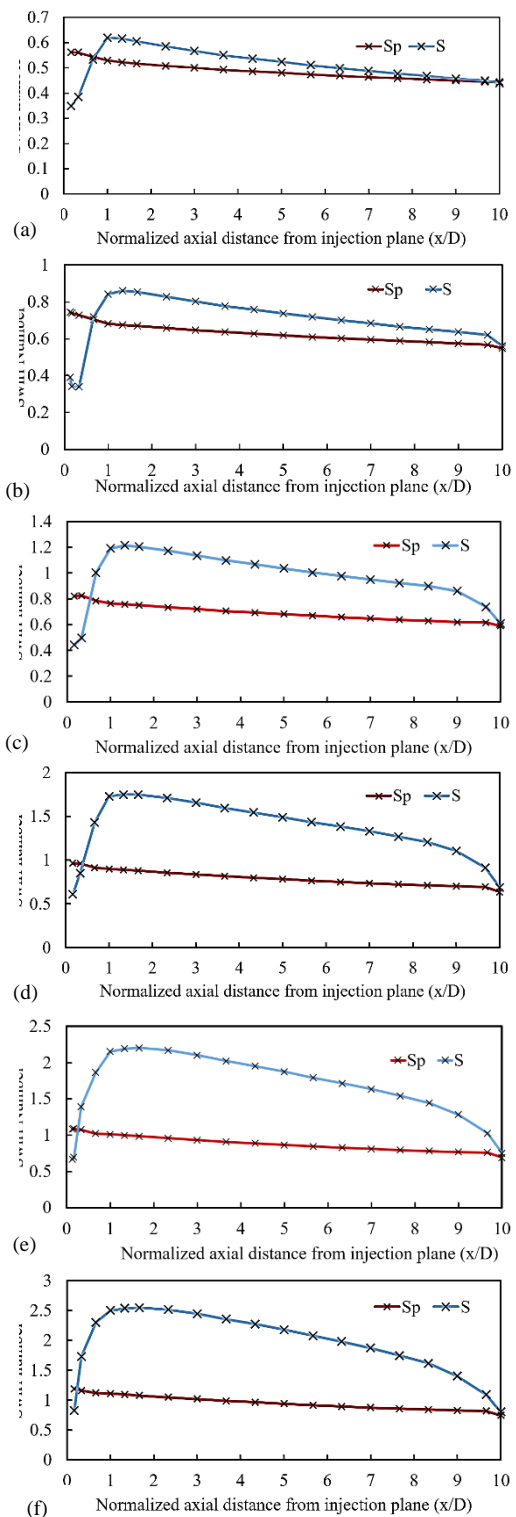


**Fig. 9: Distribution of  $S_p$  and  $S$  along with normalized axial distance for  $Re\ 71900$ , while keeping injection angle at (a)  $5^\circ$  (b)  $7^\circ$  (c)  $10^\circ$  (d)  $15^\circ$  (e)  $20^\circ$  (f)  $25^\circ$**

9, another way to characterize each case is through the corresponding maximum value attained by these Swirl Numbers, i.e.  $S_{max}$  and  $S_{p,max}$ . Fig. 10 (a) and (b) show the impact of the injection flow rate and the injection

angle on  $S_{max}$  and  $S_{P,max}$ , respectively.  $S_{max}$  and  $S_{P,max}$  both are observed to increase with the injection angle across the range of flow rates considered. Moreover, both increase sharply with flow rate at the lower flow rates and tend to asymptote towards a limiting value at the higher Re. Although the asymptotic trend is more obvious by observation in the  $S_{P,max}$  trend than the  $S_{max}$  trend for the range of Re considered, it is arguable that there exists an asymptotic value of the maximum Swirl Number, given the injection angle, as presented in Table 1.

It is generally considered a rule-of-thumb that there is IRZ formation in swirling flows in non-complex SB geometries when  $S$  exceeds 0.6 (Syred and Beer 1974; Gupta et al. 1984). Similar guidelines do not exist in the literature for the case of swirling flows in TIB configurations, as detailed in the introduction section. Accordingly, the various swirling flow cases in the TIB geometry are analysed for IRZ formation in this work based on variations in the injection angle and the flow Re.

Figure 11(a) shows the impact of these inlet boundary conditions on the IRZ length normalized by the domain diameter  $D$ . The results indicate that the IRZ or mixing zone size increases considerably with injection angle, especially above 15°. It should be noted that IRZ formation is not observed at the 5° injection angle. This is actually the reason that 5° is chosen as the lower limit of our injection angle range investigated. Vortex breakdown and IRZ initiation occur at the injection angle of 6°, which corresponds to  $S_{max}$  and  $S_{P,max}$  values of around 0.6, as observed in Table 1, and matches with the critical Swirl Number value in SB geometries (Syred and Beer 1974; Gupta et al. 1984).

It is noteworthy that while the Swirl Number for evaluating criticality depends on the inlet swirler geometry in SBs, it is the asymptotic value of  $S_{max}$  and  $S_{P,max}$  that matters in TIBs given the fact that they vary with flow Re especially at the lower Re values. Figure 11(a) also shows that the mixing zone size increases with flow Re and approaches an asymptotic value at all injection angles. Similar trends were observed in the variation of  $S_{max}$  and  $S_{P,max}$  in Fig. 10 and Table 1. Hence, each injection angle is characterized by asymptotic values of the Swirl Numbers ( $S_{max}$  or  $S_{P,max}$ ) as well as the normalized IRZ length, which are plotted against each other in Fig. 11(b).

**Table 1 Asymptotic swirl number independent of flow Reynolds number for the given injection angle and geometry.**

Injection angle ( $\alpha$ )	Asymptotic swirl number ( $S_{max}$ )	Asymptotic swirl number ( $S_{P,max}$ )
5°	0.62	0.59
6°	0.64	0.59
7°	0.74	0.64
10°	1.23	0.83
15°	1.77	0.98
20°	2.23	1.09
25°	2.58	1.19

IRZ initiation observed at 6°

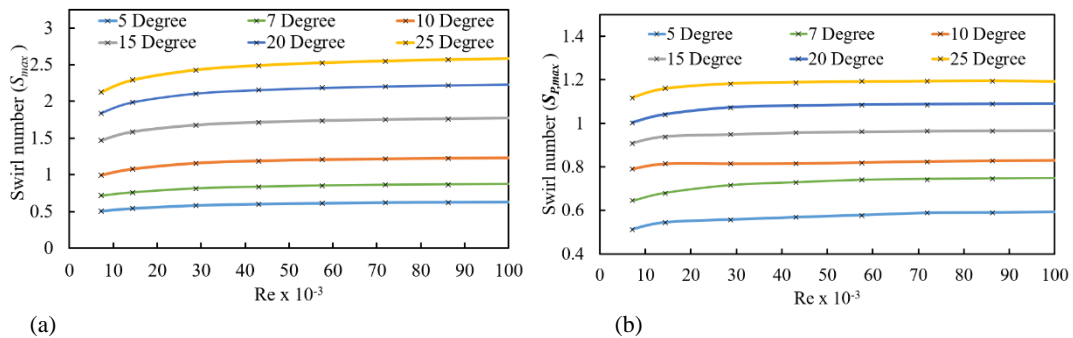


**Fig. 10. Distribution of (a)  $S_{max}$  and (b)  $S_{P,max}$  observed for all the injection flow range considered.**

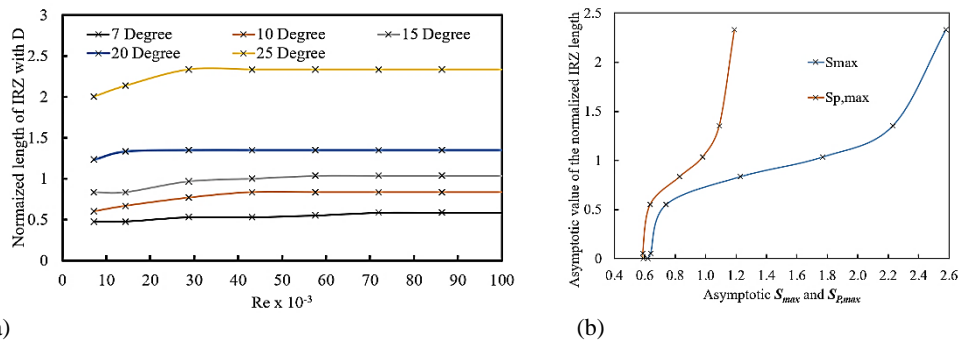
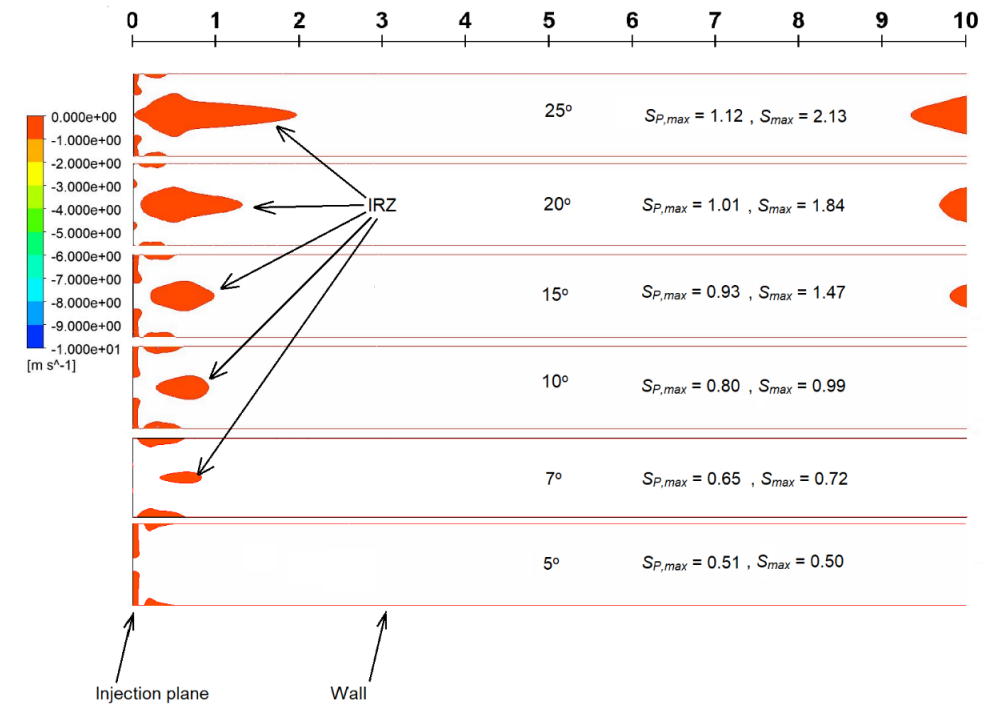
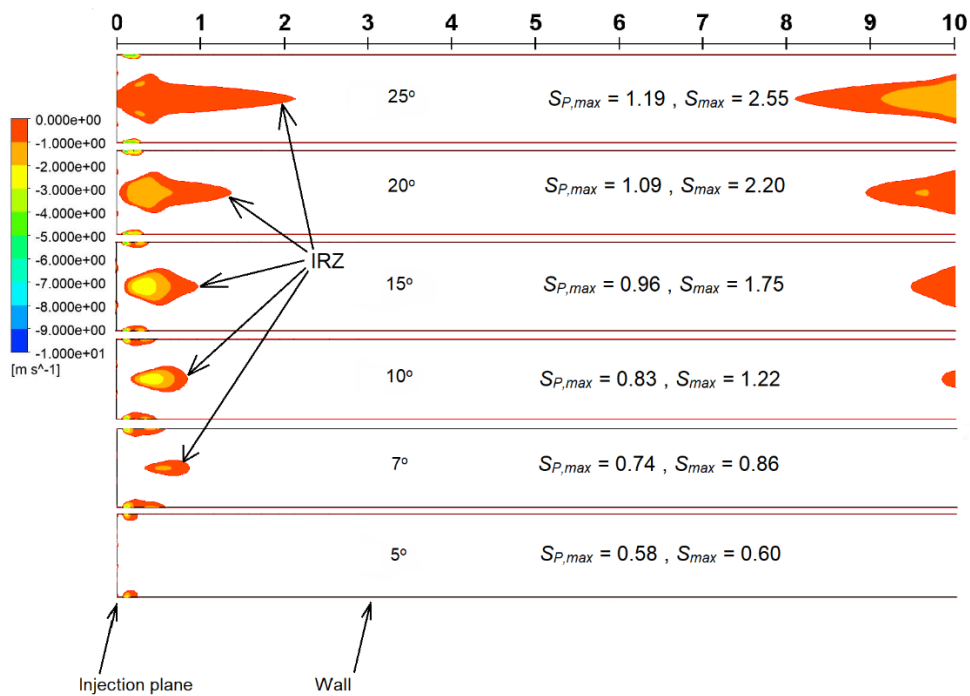


**Fig. 11. (a) Normalized IRZ Length v/s injection flow Re for various injection angles (b) Asymptotic value of the normalized IRZ length v/s corresponding asymptotic values of  $S_{max}$  and  $S_{P,max}$ .**



(a)



(b)

**Fig. 12. Contours of negative axial velocity on a central plane representing IRZ for all range of injection angle considered and corresponding asymptotic maximum swirl number ( $S_{max}$  and  $S_{P,max}$ ) for Reynolds number (a) 7190 (b) 71900.**

Figure 12 depicts the contours of negative axial velocity downstream of the injection plane on a central plane of the domain for the various injection angles considered at two different Re. The contours clearly show the IRZ formed downstream of the injection as

well as another reverse flow zone at the domain exit. The exit reverse flow zone extends more and more upstream with increasing injection angle and Re. The extent of the IRZ formed at the injection also increases with injection angle, as previously discussed. The IRZ

is expected to extend further upstream beyond the injection plane at injection angles above  $25^\circ$  based on the trends in Fig. 12. The width of the IRZ is also observed to increase with the injection angle, especially close to the injection plane. Although not included in this study, our simulations for injection angles above  $25^\circ$  show that the exit reverse flow zone extends more and more into the upstream flow and ultimately merges with the IRZ. As the current study aims to analyse the flow physics and the impact of inlet boundary conditions just downstream of the injection, hence it purposefully does not cover the cases with injection angles greater than  $25^\circ$ .

## 6. CONCLUSIONS

The present work acknowledges the fact that there is an inadequate amount of open research on the fluid dynamics of tangentially injected swirling flows. The study takes the example of a simple cylindrical geometry to focus on such flows and validates the CFD model on a swirl burner (SB) case. The validated model is then utilized to investigate the flow phenomena in cold tangentially injected flows, including the evolution of the swirl intensity and its relationship with the extent of the IRZ, for a range of tangential inlet boundary conditions. Our model and simulations support the following major findings

- The local swirl intensity ( $S$ ) downstream of the injection plane is observed to rapidly shoot up followed by gradual decay. On the other hand, the local swirl intensity modified for pressure ( $S_P$ ), undergoes a constant gradual decay downstream of the injection till the domain exit. This is because the variations in pressure and axial momentum nullify each other in the  $S_P$  expression. Hence,  $S_P$  provides a contrasting and arguably better alternative for defining the Swirl strength in comparison with the most commonly used Swirl Number  $S$ .
- The maximum values of these two Swirl Numbers attained in the domain,  $S_{max}$  and  $S_{P,max}$ , increase with the injection angle. On the other hand,  $S_{max}$  and  $S_{P,max}$  tend to asymptote with increase in bulk flow Reynolds number ( $Re$ ) for a given injection angle.
- The size of IRZ increases remarkably with the injection angle. A higher injection angle broadens the IRZ near the injection plane and elongates it further downstream. The IRZ size also increases with  $Re$  at lower values and tends to asymptote at higher values.
- The IRZ is not observed at any  $Re$  for injection angles below  $6^\circ$ . The asymptotic values of the two Swirl Numbers ( $S_{max}$  and  $S_{P,max}$ ) for the transition case are 0.64 and 0.59, respectively, hence close enough to the critical inlet Swirl Number value of 0.6 for vortex breakdown and IRZ initiation in SBs.

It is expected that the findings from the present study will aid in further optimizing the designs of TIBs, especially when it comes to the role of the IRZ in mixing and overall reactor performance. Future work should focus on extending the present analysis to reacting flows and investigating the various flow

regimes and the corresponding flow field transitions therein.

## INNOVATION STATEMENT

The manuscript challenges the use of most common Swirl Number expression, evaluated without incorporating gauge pressure to characterize the Swirl strength, and proposes implementation of an alternative definition.

## ETHICAL STATEMENT

Funding agency: The work is not funded by an external agency. It is supported by the Department of Mechanical Engineering at IIT Delhi.

Conflict of interest: Authors certify no affiliations with or involvement in any organization or entity with any financial interest or non-financial interest in the subject matter or materials discussed in this manuscript.

Ethical approval: The manuscript includes proper acknowledgement when citing our peers' work.

Informed consent: Authors have not involved any human participants to conduct research.

Author contributions: Study was conceptualized by MK. Preparation, collection and analysis of data was performed by RS. The first draft of manuscript was written by RS and edited into the final version by MK. All authors read and approved the final manuscript.

## REFERENCES

- Ahmed, S. A. (1998). Velocity measurements and turbulence statistics of a confined isothermal swirling flow. *Experimental Thermal and Fluid Science* 17(3), 256-264.
- Ahmed, S. A. and A. S. Nejad (1992). Velocity measurements in a research combustor part 1: Isothermal swirling flow. *Experimental Thermal and Fluid Science* 5(2), 162-174.
- Ahmed, S. A. and A. S. Nejad (no date) *Experimental data repository, European Research Community on Flow, Turbulence and Combustion*. Available at: <http://cfm.mace.manchester.ac.uk/ercoftac/doku.php?id=cases:case001>.
- Al-Abdeli, Y. M. and A. R. Masri (2015). Review of laboratory swirl burners and experiments for model validation. *Experimental Thermal and Fluid Science* 69, 178-196.
- Alekseenko, S. V., P. A. Kuibin, V. L. Okulov and S. I. Shtork (1999). Helical vortices in swirl flow. *Journal of Fluid Mechanics* 382, 195-243.
- Anacleto, P. M., E. C. Fernandes, M. V. Heitor and S. I. Shtork (2003). Swirl flow structure and flame characteristics in a model lean premixed combustor. *Combustion Science and Technology* 175(8), 1369-1388.
- Beér, J. M., J. Chomiak and L. D. Smoot (1984). Fluid dynamics of coal combustion: A review. *Progress in Energy and Combustion Science*

- 10(2), 177-208.
- Benesch, W. and H. Kremer (1985). Mathematical modelling of fluid flow and mixing in tangentially fired furnaces. *Symposium (International) on Combustion* 20(1), 549-557.
- Bezaatpour, M. and M. Goharkhah (2020). Convective heat transfer enhancement in a double pipe mini heat exchanger by magnetic field induced swirling flow. *Applied Thermal Engineering* 167, 114801.
- Boushaki, T., A. Koched, Z. Mansouri and F. Lespinasse (2017). Volumetric velocity measurements (V3V) on turbulent swirling flows. *Flow Measurement and Instrumentation* 54, 46-55.
- Brown, G. L. and J. M. Lopez (1990a). Axisymmetric vortex breakdown part 1. Confined swirling flow. *Journal of Fluid Mechanics* 221, 553-576.
- Brown, G. L. and J. M. Lopez (1990b). Axisymmetric vortex breakdown part 2. physical mechanisms. *Journal of Fluid Mechanics* 221, 553-576.
- Cary, A. W. and D. L. Darmofal (2003). Axisymmetric and Non-Axisymmetric initiation of vortex breakdown. 069, 1-23.
- Chen, S., B. He, D. He, Y. Cao, G. Ding, X. Liu, Z. Duan, X. Zhang, J. Song and X. Li (2017). Numerical investigations on different tangential arrangements of burners for a 600MW utility boiler. *Energy* 122, 287-300.
- Doherty, T. O. (2001). Vortex breakdown: a review. *Progress in Energy and Combustion Science* 27, 431-481.
- Escudier, M. P. (1984). Observations of the flow produced in a cylindrical container by a rotating endwall. *Experiments in Fluids* 2(4), 189-196.
- Escudier, M. P., J. Bornstein and N. Zehnder (1980). Observations and LDA measurements of confined turbulent vortex flow. *Journal of Fluid Mechanics* 98(1), 49-63.
- Gaikwad, P., H. Kulkarni and S. Sreedhara (2017). Simplified numerical modelling of oxy-fuel combustion of pulverized coal in a swirl burner. *Applied Thermal Engineering* 124, 734-745.
- Gerz, T. and T. Ehret (1997). Wingtip Vortices and Exhaust Jets during the Jet Regime of Aircraft Wakes. *Aerospace Science and Technology* 1(7), 463-474.
- Gupta, A., D. G. Lilley and N. Syred (1984) *Swirl Flows*, Abacus Press.
- Harvey, J. K. (1962). Some observations of the vortex breakdown phenomenon. *Journal of Fluid Mechanics* 14(4), 585-592.
- Ko, J. (2005). *Numerical Modelling of Highly Swirling Flows in a Cylindrical Through-Flow Hydrocyclone*. Thesis, Royal Institute of Technology, Sweden.
- Mansouri, Z. and T. Boushaki (2018). Experimental and numerical investigation of turbulent isothermal and reacting flows in a non-premixed swirl burner. *International Journal of Heat and Fluid Flow* 72, 200-213.
- Serre, E. and P. Bontoux (2002). Vortex breakdown in a three-dimensional swirling flow. *Journal of Fluid Mechanics* 459, 347-370.
- Stone, C. and S. Menon (2001). Combustion Instabilities in Swirling Flows. In *37th Joint Propulsion Conference and Exhibit*, Salt Lake City, UT, U.S.A.
- Syred, N. and J. M. Beer (1974). Combustion in swirling flows: a review. *Combustion and Flame* 20(2), 143-201.
- Villasenor, R. and R. Escalera (1998). A highly radiative combustion chamber for heavy fuel oil combustion. *International Journal of Heat and Mass Transfer* 41(20), 3087-3097.
- Wang, P., X. S. Bai, M. Wessman and J. Klingmann (2004). Large eddy simulation and experimental studies of a confined turbulent swirling flow. *Physics of Fluids* 16(9) 3306-3324.
- Wang, Y., X. Wang and V. Yang (2018). Evolution and transition mechanisms of internal swirling flows with tangential entry. *Physics of Fluids* 30(1), 013601.
- Wang, Y. and V. Yang (2018). Central recirculation zones and instability waves in internal swirling flows with an annular entry. *Physics of Fluids* 30(1), 013602.
- Weber, R., B. M. Visser and F. Boysan (1990). Assessment of turbulence modeling for engineering prediction of swirling vortices in the near burner zone. *International Journal of Heat and Fluid Flow* 11(3), 225-235.
- Xia, J. L., G. Yadigaroglu, Y. S. Liu, J. Schmidli and B. L. Smith (1998). Numerical and experimental study of swirling flow in a model combustor. *International Journal of Heat and Mass Transfer* 41(11), 1485-1491.
- Zhao, B., Y. Ren, D. Gao and L. Xu (2019). Performance ratio prediction of photovoltaic pumping system based on grey clustering and second curvelet neural network. *Energy* 171, 360-371.
- Zhao, B., H. Chen, D. Gao and L. Xu (2020). Risk assessment of refinery unit maintenance based on fuzzy second generation curvelet neural network. *Alexandria Engineering Journal* 59(3), 1823-1831.
- Zhao, B. and H. Song (2021). Fuzzy Shannon wavelet finite element methodology of coupled heat transfer analysis for clearance leakage flow of single screw compressor. *Engineering with Computers* 37(3), 2493-2503.